Analysis of GOME stray light

R.M. Koopman European Space Agency; ESA/ESRIN Via Galileo Galilei C.P. 64, 00044 Frascati, Italy
Rob.Koopman esrin.esa.it
http://www.cs.esrin.esa.it/

Abstract

A study of stray light that reaches the detectors of the Global Ozone Monitoring Experiment (GOME) is presented. GOME was designed to have direct stray-light detection capabilities, which have been used for this study. Stray light is measured when the instrument observes the sun, the moon, the earth and the on-board calibration lamp. Level0 and Level1 GOME data are used to refine the characterisation of the stray light, and identify peculiar features that are present in one or more of these observation modes.

Keywords: GOME, stray light, calibration

Introduction

The Global Ozone Monitoring Experiment is a high-resolution spectrometer launched on ERS2. It is the first space-bourne instrument to use the Differential Optical Absorption Spectroscopy (DOAS) technique to derive total column amounts of several atmospheric trace gasses, among which notably Ozone and NO_2. Currently, O_3 and NO_2 columns are provided operationally as Level 2 products, whilst prototype processors, using Level 1 products (calibrated radiance and irradiance spectra), have already produced Ozone profiles reaching down into the Troposphere. Both the Level 2 DOAS product and especially the profiles are dependent on the quality of the Level 1 product. Correction for stray light is mandatory for obtaining accurate radiance and irradiance spectra. Level 1 and Level 2 products are generated by the Deutsche Forschungsanstalt für Luft- und Raumfahrt (DLR) on behalf of the European Space Agency (ESA), using level 0 data from ESA as input. A stray-light correction algorithm is included in the GOME Data Processor (GDP) using fixed values for the stray light.

The Global Ozone Monitoring Experiment (GOME)

The GOME spectrometer has a spectral coverage that ranges from 240 to 790 nm distributed over 4 detectors, with a resolution that varies from 0.2 to 0.4 nm. Each detector contains 1024 diodes, most of which are directly illuminated by the radiation source. This source can be the earth (atmosphere), the Sun, the Moon, and the on-board calibration lamp. Several diodes are outside the path of the light source, and among them are the diodes of the so called stray-light bands.

Detector band	start pixel	# of pixels
Blind 1a	0	49
Stray 1a	206	50
Band 1a	256	625
Band 1b	881	70
Stray 1b	951	50
Stray 2a	133	50
Band 2a	183	8
Band 2b	192	831
Channel 3	0	1024
Channel 4	0	1024

Table 1: Detector pixels

Data from the three stray-light bands have been used for this study, and combined with data from Bands 1A, 1B, 2A and 2B. Level 1 data files have been used for Earth, Sun and Moon observations, Level 2 data have been used for Lamp and Dark signal measurements and for verification of Level 1 data. Level 2 data have been used, among others, to test for correlations with cloud-cover fraction. Since pre-flight calibration had demonstrated that inter-channel stray light is negligible, this study focusses on intra-channel stray light. Intra-channel stray light consists of contributions from uniform stray light and ghost stray light. In-flight measurements show evidence that parts of the stray-light bands are actually not perfectly shielded from direct radiation.

Contamination of stray-light bands

Figure 1 shows that, in the stray-light bands of detector **1**, the distribution of intensities within the stray-light bands 1A and 1B changes in a non-uniform manner in the parts of the bands closest to the directly-illuminated part of the detector. These parts of the detector suffer from contamination by direct illumination to such an extent that they cannot be used for determination of stray-light levels.

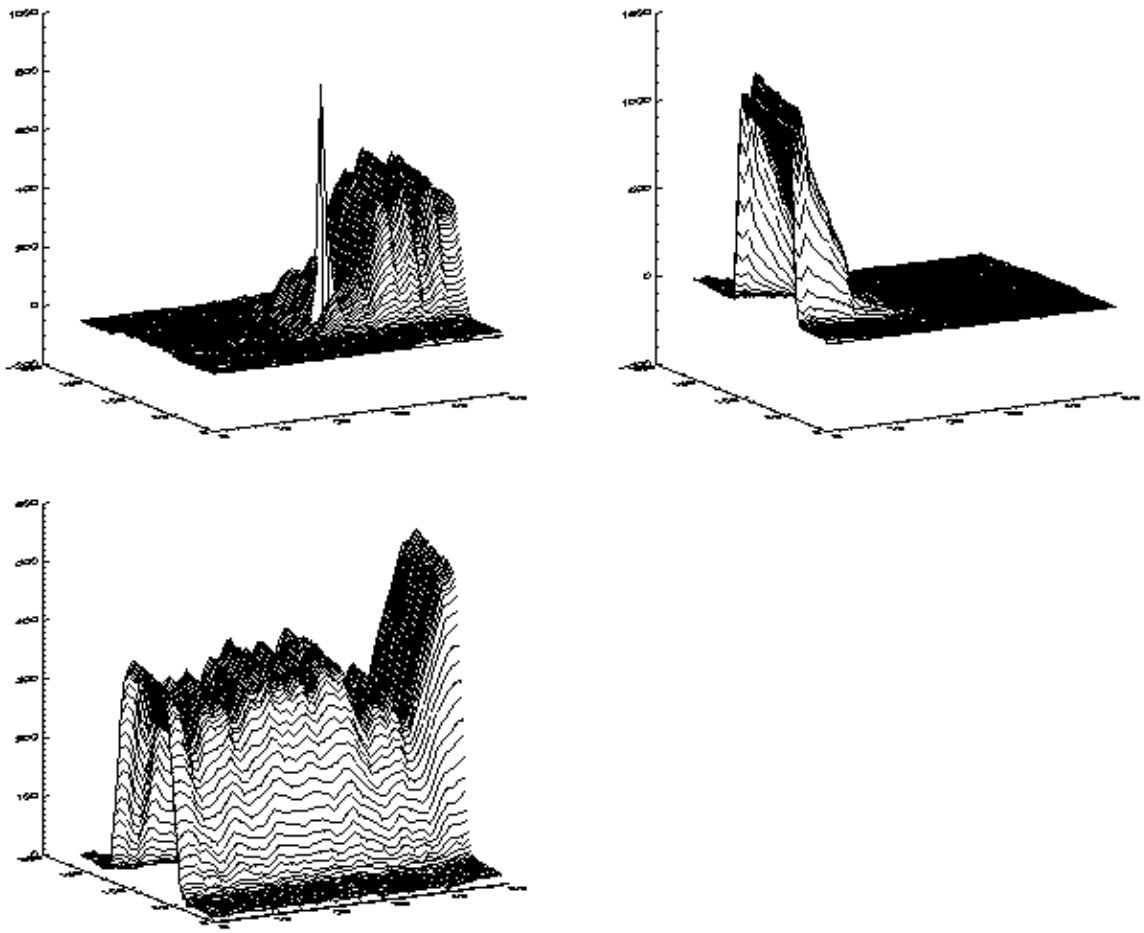

Figure 1: Signal in stray-light bands 1A, 1B and 2A during solar calibration (X: pixel nr, Y: product nr, Z: signal [BU]).

The more complicated pattern for stray-light band 2A can be explained by assuming that the entire band suffers from contamination by direct illumination. Evidence for this is presented in Figure 2, by using an extrapolated wavelength calibration (GDP lv1) which includes the pixels of the stray-light bands, and subsequently comparing the stray-light pattern with a SOLSTICE solar spectrum (Peeters,P.). Considering the difference in wavelength resolution between the two instruments, the correspondence is sufficiently evident to conclude that the entire stray-light band 2A is contaminated by direct illumination. It will be shown hereafter that consolation for this loss can be found in the use of the contaminated regions for improvement of the wavelength calibration. The Fraunhofer structure in Stray 2A has also been identified in Moon observation data.

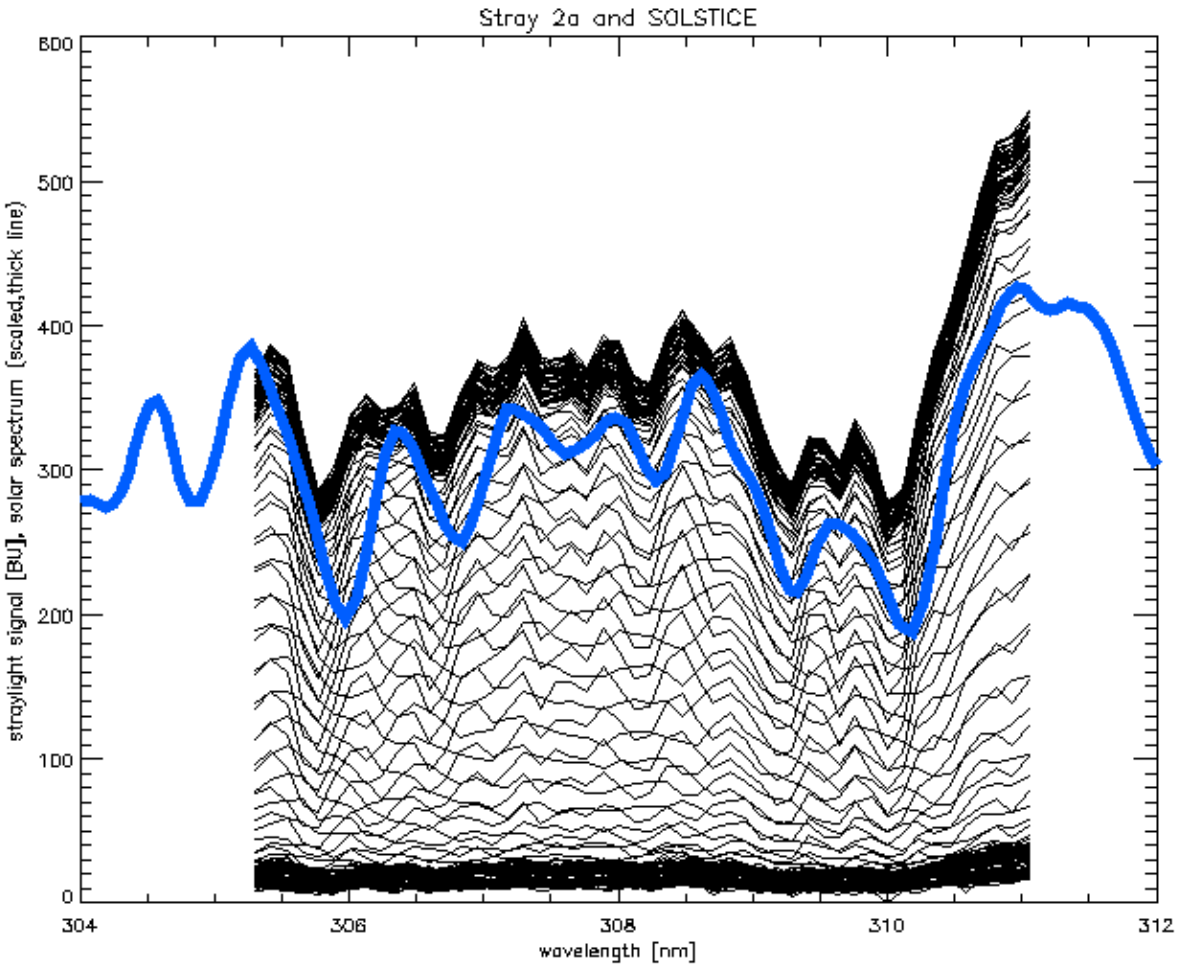

Figure 2: Comparison of stray light 2A with a SOLSTICE spectrum (blue line). The wavelength values for the pixels of the stray-light band are an extrapolation of those for the pixels of Band 2A and 2B. Please note that the wavelength resolution of GOME is higher than the resolution of SOLSTICE in this wavelength region.

Stray-light fraction

Uniform intra-channel stray light can be characterised by the straylight fraction per pixel *F*. For this purpose, GDP level 1 data have been extracted applying correction for dark current, fixed pixel-to-pixel gain and Peltier-cooler control-loop cross-talk (options **L**,**A**, **F** of the **gdp01_ex** extraction programme provided by DLR) Only first 11 pixels of stray-light band 1A and the last 11 pixels of stray-light band 1B have been included in order to avoid the contaminated regions. Numerical values for the stray-light fraction have been calculated and an example is shown in Figure 3 for Sun and Moon measurements and in Figure 7 for Earth observations.

$$F = \frac{\text{average signal of straylight pixel per unit time}}{\text{average signal band 1A and B pixel per unit time}}$$

Correction is made for the difference in integration time for Band 1A and Stray 1A on the one hand (1.5 seconds), and Band 1B and Stray 1B on the other hand (0.75 seconds) during Sun Calibration. Band 1B integrates only during the second half of the integration of Band 1A, consequently they do not see the same scene. When the sun enters the field of view, Band 1B only samples the brightest part of the integration of Band 1A and the opposite is true when the Sun exits from the field of view. This explains the hysteresis seen in Figure 3 (Caspar,C.). For Sun measurements the fraction *F* agrees with that used in the GDP (*F* = 0.02),although for the single Moon observation evaluated thus far, a much higher value *F* = 0.01 is found.

The large difference in stray-light fraction between sun and moon observations can partially be attributed to an inadequate correction for cross-talk during Moon measurements. As shown in figure Figure 4, Peltier-cooler control-loop cross-talk correction does not suffice to remove a semi-periodic oscillation from the moon signal in Channel 1 and 2. Since the Moon signal also has a time dependence, since the Moon passes through the field of view of the instrument slit, these oscillations directly affect the slope *F* of the plot in Figure 3. The amplitude of the oscillations is reaches values of up to 50% of the maximum signal in the stray-light bands during Moon measurement, and is thus sufficient to significantly affect the results of the stray-light fraction calculations.

The calculation of stray-light fraction for Earth-shine measurements in Figure 7 indicates that stray light is extremely noisy for the Nominal-Observation Time line, to such an extent that the stray-light fraction found is of limited significance.

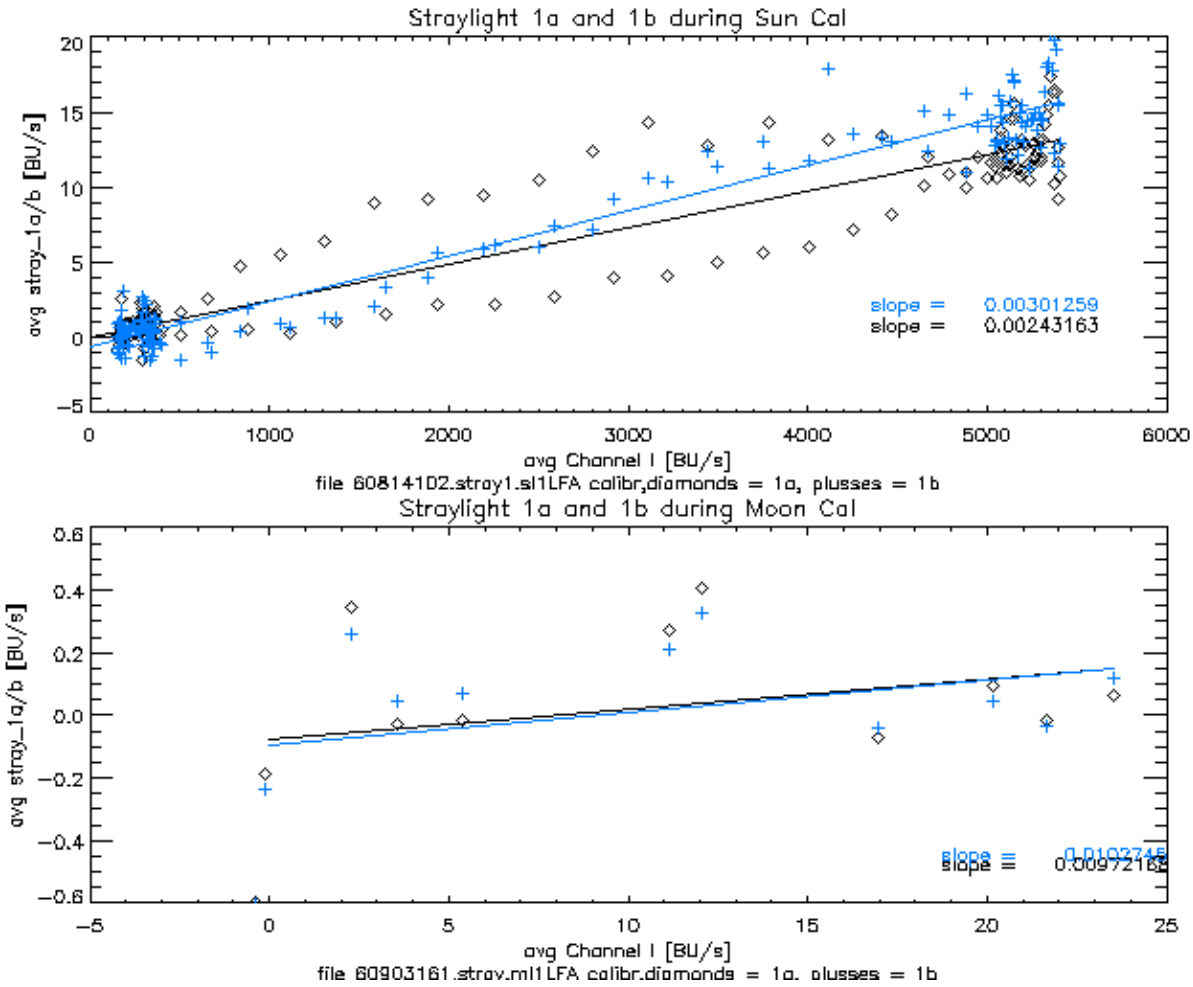

Figure 3: Relation between stray-light level and total signal in Channel 1. Top plot displays results Sun calibration, bottom plot for Moon measurement. "slope" is the stray-light fraction F.

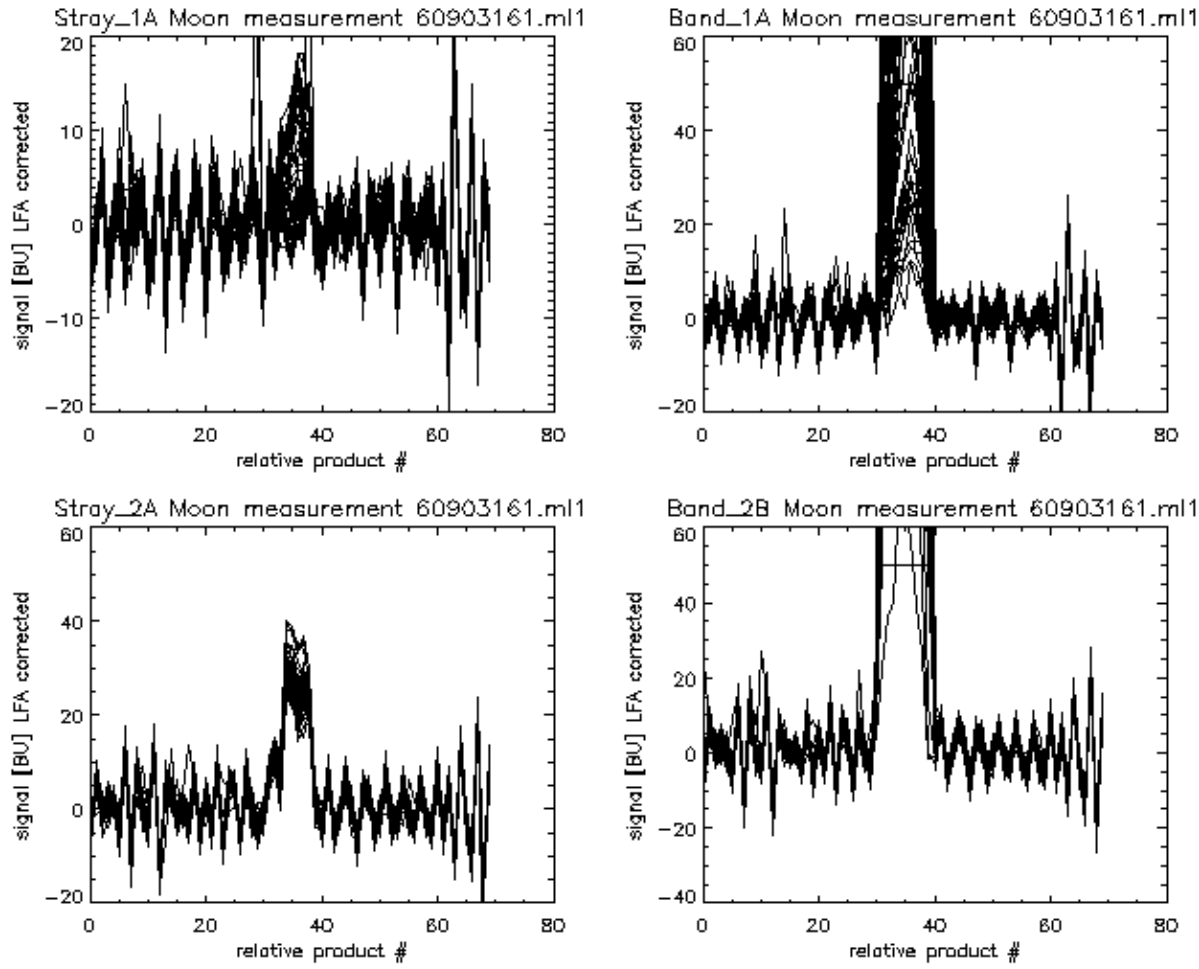

Figure 4: Time dependence of detector signal during Moon measurement. Although the Peltier-cooler cross-talk correction option was applied during extraction, a strong time-dependent oscillation remains in the signal. These remaining variations still display the signature of Peltier-type cross-talk, among others the identical phase for all bands within one channel and an oscillation period in the order of 60 seconds (The integration time for these Moon measurements is 12 seconds).

Pixel-dependent time lags

During the investigation of stray light, the phenomenon of time delays, previously reported by Slijkhuis,S., 1995 became apparent. When the sun enters the field of view of the detector, it is expected that all detector pixels commence to detect an increase in signal at almost the same time. The sequential read-out of detector pixels can only cause slight differences between pixels of 91.55 µs. The integration of pixel #0 (shortest wavelength) reaches completion 93.75 ms after the end of integration of pixel #1023. In Figure 5 it can be seen that time delays of the onset of the rise in intensity (and with it the onset of the flattening of the intensity curve, and the onset of the decent) are several orders of magnitude larger (10 seconds) than can be explained by sequential readout (maximally 93.75 ms). Moreover, the delays do not increase linearly with pixel number.

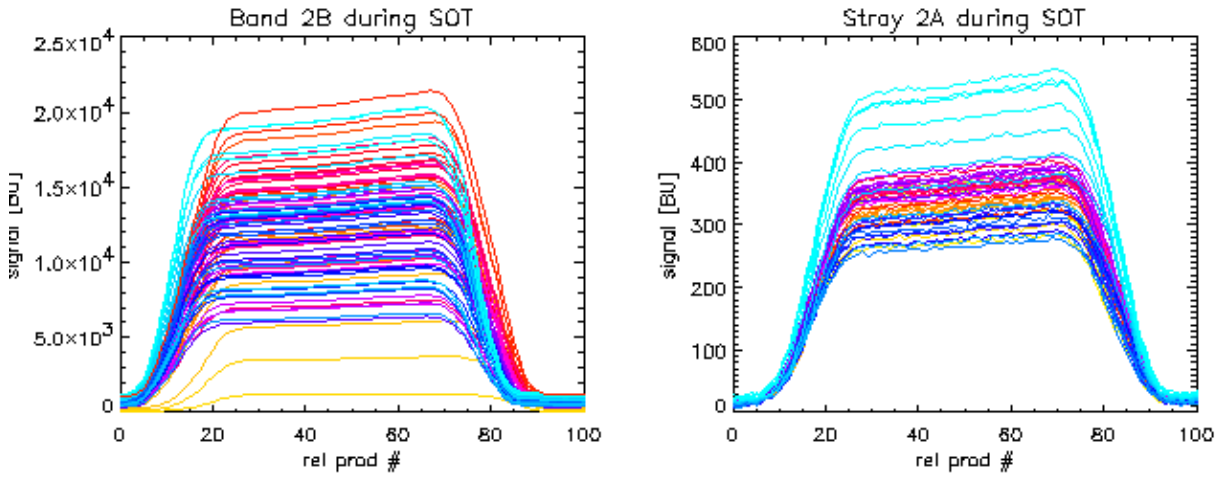

Figure 5: Time dependence of Solar calibration.
Each line represents the signal of one detector pixel as a function of time

(product number). The darkest-blue line represents pixel #0 and the darkest-red line represents pixel #830 for Band 2B and pixel # 49 for Stray 2B. A time lag between the different pixels is evident, and this time lag does not vary linearly with pixel number.

To further characterise this phenomenon, for each pixel the signal was normalised through division by its value in a product close to maximum. The resulting time dependence of this normalised Sun measurement is shown in Figure 6, colors representing intensity. Particularly striking is the delay pattern in stray-light band 1B (Stray 1B), where the directly illuminated part of the band displays a continuation of the behaviour of Band 1B, whereas the outer pixels of Stray 1B have a lag that corresponds with the timing of the central pixels of Band 2B. For pure stray light, this latter type of behaviour is consistent, since these central pixels contribute most to the total signal in the Bands, and thus also to pure stray light. So although the cause of the time lags is yet uncertain, the fact that the lags of the brightest pixels and the outer 1B stray-light pixels are similar confirms that the latter are indeed sensitive to stray light.

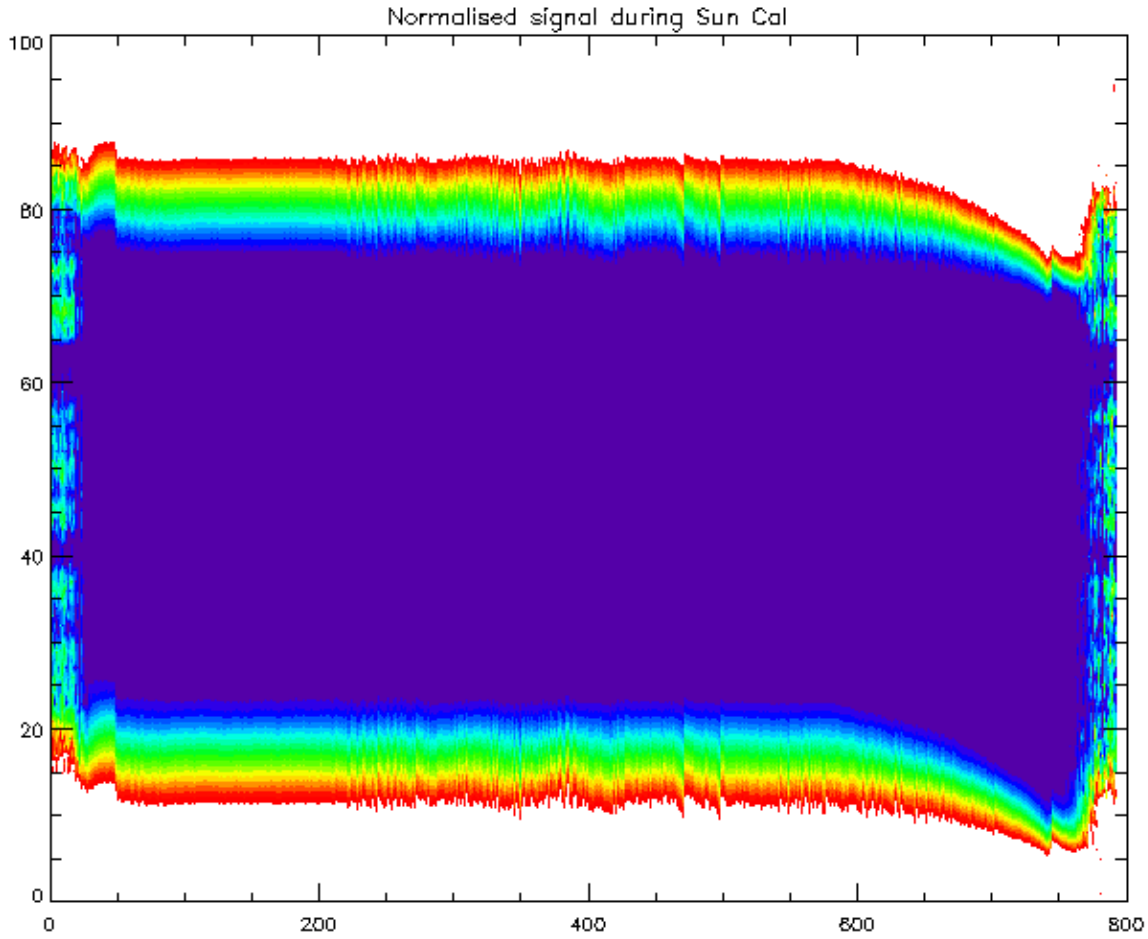

Figure 6: time dependence of normalised signal in Channel 1 during Sun calibration. The curves in Figure 5 have been normalised and the signal (Y direction in Figure 5) is now represented by color values. The interval between products is 1.5 seconds (even though the integration time in Band 1B is 0.75 seconds). All pixels of Stray 1A (0:49), Band1A (50:674), Band 1B (675:744) and Stray 1B (745:794) are represented.

Moon measurements were studied as well, in order to further characterise this phenomenon, but identification of potential time lags proves more difficult because the long integration time (12 seconds, which is similar to the maximum time lag found in solar observations), the lower intensity and hence greater relative noise level, and also because of the cross-talk oscillation which has a significant amplitude compared to the rise and decent of the Moon signal in the low-intensity parts of the spectrum.

Dark-signal correction

Earth-shine level 1 data often contain negative values for stray light, which is obviously unphysical. An example is presented in Figure 7, where negative stray-light values are found even for high intensities in Bands 1A and 1B. A likely cause for negative signals is excessive correction, notably dark-signal correction. The orbit in Figure 7 passes over the South Atlantic Anomaly (SAA) during dark-signal calibration.

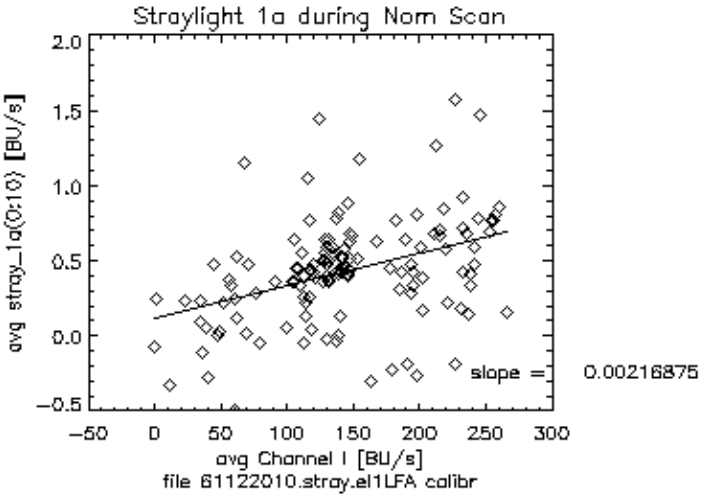

Figure 7:

Two to three orbits per day pass over the SAA on their descending node, and are affected by spikes in the measurements, but another three orbits pass over the SAA during their ascending node, and potentially the dark-signal measurements can occur whilst the instrument passes through the SAA. In Figure 8, the signal in Band 1A is shown, during the interval in which the instrument passes through the SAA. Within the SAA the dark current increased from typically 4 BU/s to a peak value of 15 BU/s. Calculation of dark current using these measurements inside the SAA will result in overestimation. Application of excessive dark-current correction during extraction of level-1 data will lead to the negative values which have been actually been observed in **several** data files. The variation of dark signal within the SAA is sufficiently gradual and regular to render automatic detection and exclusion a feasible option for ground processing/data extraction.

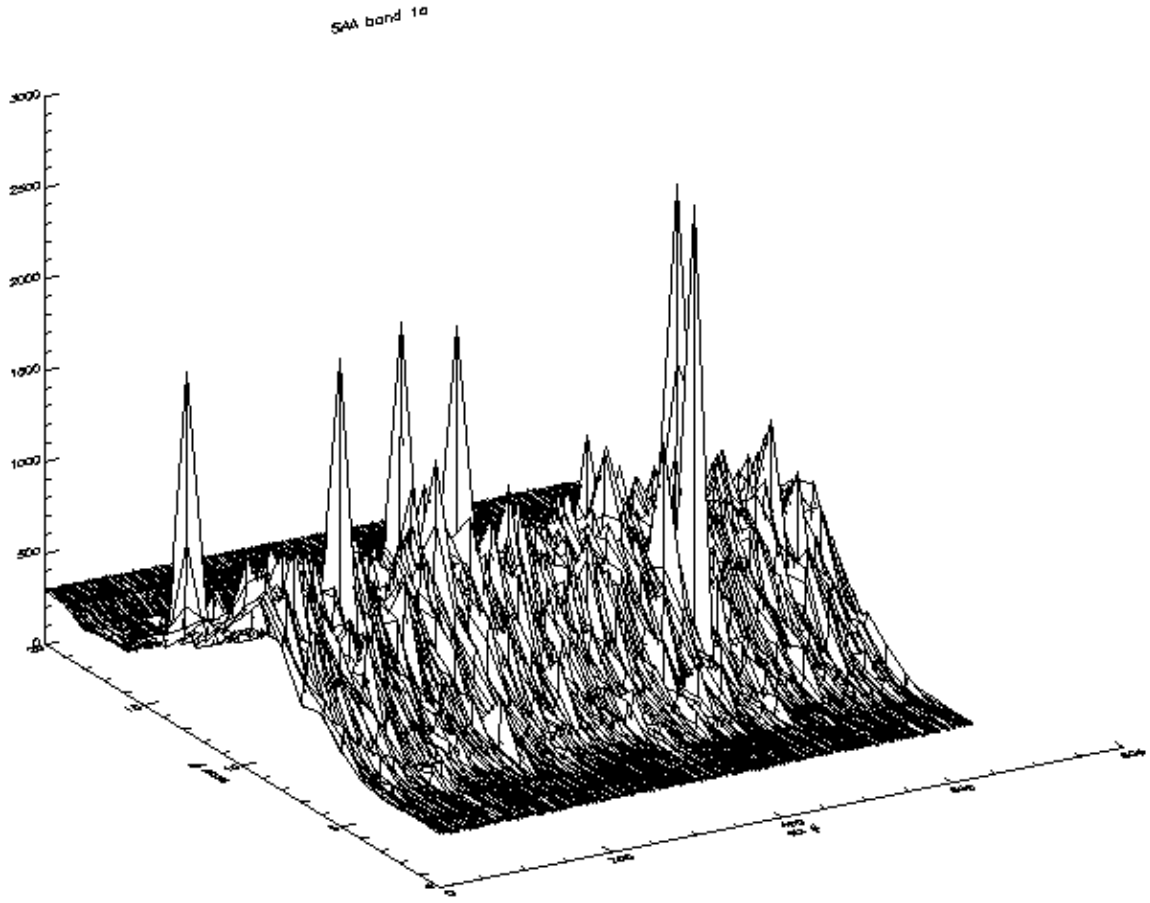

Figure 8: Signal in Band 1A during passage through the SAA. Integration time in Band 1A during these measurements was 60 seconds. Spikes are frequent enough to cause a rise of the entire base level.

Lamp lines in contaminated parts of stray-light bands

Extracted GOME Calibration Data (EGOC) were used to analyse stray light during lamp measurements. Strong emission line features were found in stray light bands. Although ghost lines are to be expected in stray-light bands, the previous evidence of partial direct illumination suggests that these lines could also be due to direct illumination. The **gdp01_ex** extraction programme provides an extrapolation of the wavelength calibration into the stray-light bands, so that for each pixel of the band, a wavelength value is available corresponding to direct illumination. An atlas of the spectrum of the on-board calibration lamp (Murray, J. E.,

1995)was used to test for each line found in the stray-light bands whether it can be due to direct illumination or whether it could be a ghost line, reflected relative to the ghost symmetry pixels in the channel.

In stray-light band 2A only one line is present, at pixel #9 which perfectly matches the expected position of a lamp line at 306.4 nm.
Extrapolated wavelength information is available for stray-light band 1A but the atlas contains no information for wavelengths below 240 nm, hence the lines in this band could not yet be identified as due to direct illumination. They are unlikely to be ghost lines, since no lines were found at locations corresponding to reflection with respect to the pixel of symmetry, i.e. detector pixel #448.
Several lines are present in stray-light band 1B, and comparison with the atlas shows that the distribution pattern partially matches that of the lamp, but is shifted by 1.5 pixel. Even assuming non-optimal wavelength calibration and accepting lines within 2 pixels of their calculated position, unidentified features remain. Identification as (intra-channel) ghost lines has not yet been possible due to absence of an atlas covering the sub-240 nm wavelength region. Identification of lamp lines in the long-wavelength part of Band 1B has revealed that there too the wavelength calibration seems not optimal, resulting in differences of about one pixel.

Lamp-line evolution

After definitive identification of time lags in the solar calibration, and their tentative identification during moon measurements, lamp calibration measurements also have been subject of such investigation. The time-dependence of the lamp signal is shown in Figure 9 for two lamp measurements sandwitching a sun calibration measurement. The absence of a time lag in the onset of the rise of the signal is evident, but another phenomenon appears. The red circle isolates a region where a line that initially is slightly less intense than a line of similar intensity, slowly becomes more intense in the course of time. The pattern repeats itself perfectly during the second calibration measurement.

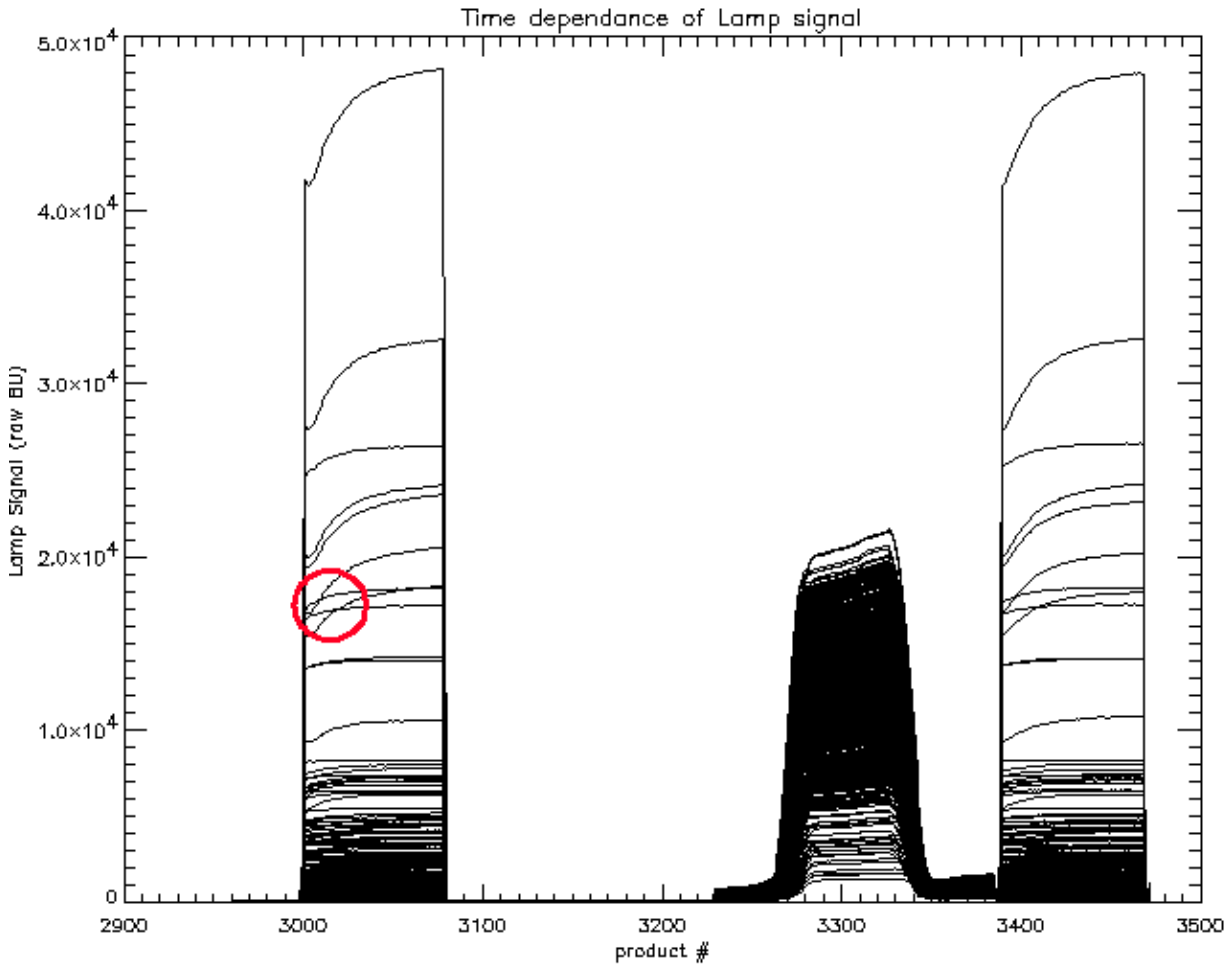

Figure 9: Time dependence of the intensity of lamp lines. Lamp measurements taken before and after sun measurement are shown as a function of time. Each line represents the signal for an individual detector pixel. Whereas for the sun observation the signal in all pixels follows the same curve with different time lags, the time lags are absent for the lamp measurements. During lamp measurements, the signals do not follow identical curves for all pixels.

This diffence in time dependence of line intensities could be correlated neither with lamp intensity itself, nor with line width, nor with position in the detector array (pixel number) A striking example has been selected for depiction in Figure 10. Two adjacent lines of identical intensity are shown, of which only one shows a time dependence. No correlation was found with the distribution of time lags over pixels, as found during sun and moon observations, hence the phenomenon is most likely to originate from the lamp itself. When weak lines are used for wavelength calibration, it is advisable to use the data products taken shortly before lamp switch off, and monitor this phenomenon during the life time of the lamp.

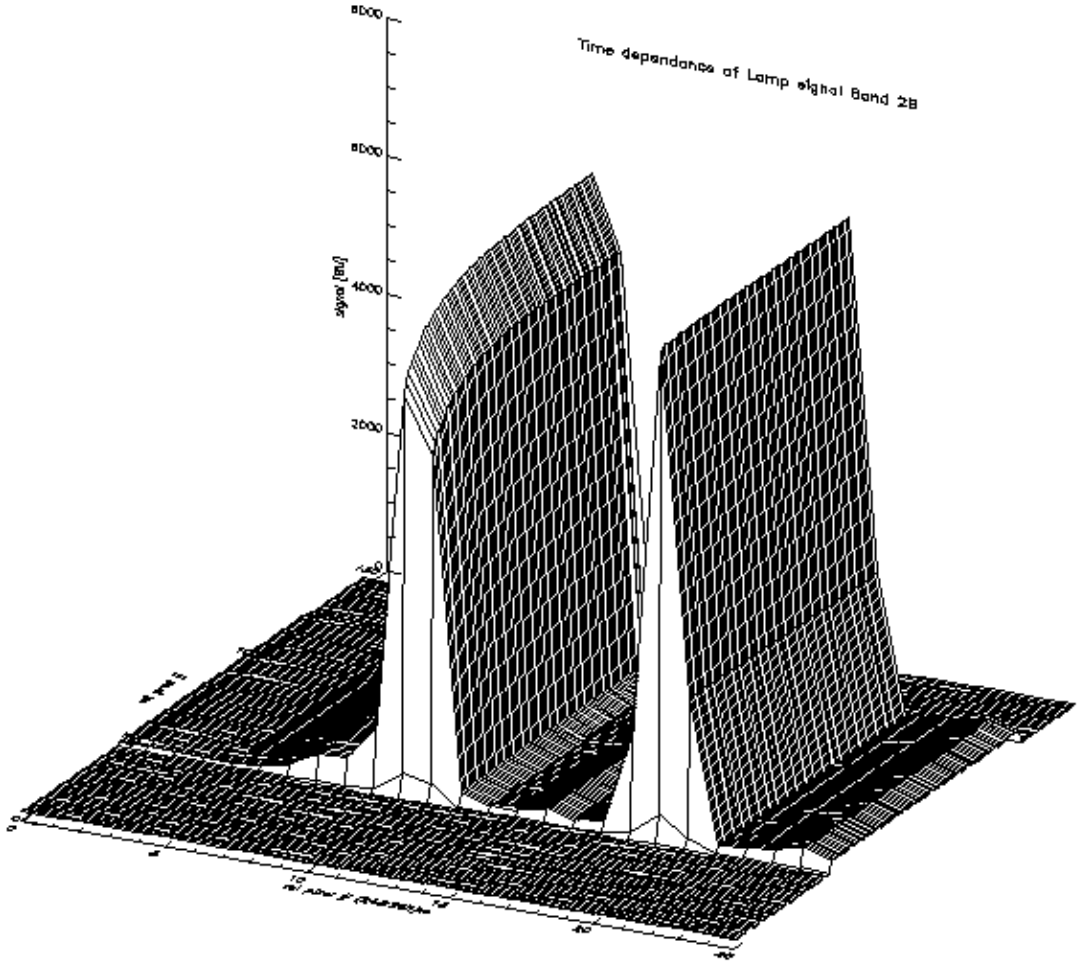

Figure 10:

The absense of time lags in the lamp data provides additional information on the time lags found during solar calibration. Since the light paths between scan mirror and detector are the same for sun and lamp measurements, the phenomenon is most likely related to the partial filling of the slit. The vertical Field of View (FoV) was already shown to be wavelenght dependent (TPD document, 1994), but for channel 2, this dependence is nearly linear with pixel number, unlike the pattern found for the time lags. The non-linearity of the time lags does not provide support to the hypothesis of detector misalignment.

Recommendations

Although the stray-light fractions derived for solar observations match the value used in the GOME Data Processor, the analysis of the sensitivity of the GOME detectors to stray light leads to several recommendations to the parties involved in calibration of the GOME FM and BBM, and GOME Data Processing:

Avoid using stray-light band 2A for any stray-light correction calculations.
Consider the use lamp lines in stray-light band 2B to improve the wavelength calibration at the long-wavelenght part of Band 2B.
Improve dark signal corrections to avoid unphysical radiance values.
In particular, avoid the use of dark signal measurements collected whilst traversing the SAA for correction calculations.
Improve the Peltier-cooler control-loop cross-talk correction for moon observations.
Use preferably only the lamp measurements shortly before lamp switch off.
Consider to determine the spectrum of the calibration lamp below 240 nm. If the lines found in this region are not ghost lines, there is the potential to use them for improvement of wavelength calibration.

Acknowledgements

The author is particularly grateful to Christophe Caspar (ESA/ESTEC), Sander Slijkhuis (DLR), Claus Zehner (ESA/ESRIN) and Achim Hahne (ESA/ESTEC) for their valuable suggestions, and Philippe Peeters (BISA) for making available a solar spectrum from SOLSTICE.

References

Slijkhuis,S., 1995
Minutes of the 18th GOME Data and Algorithm Subgroup Meeting, Annex A.

Peeters,P.,
private communication/file transfer, normalised SOLSTICE spectrum, 14 Aug 1996, level 3BS version 9.

Caspar,C.
Private communication.

Murray, J. E., 1995
Atlas of the Spectrum of a Platinum/Chromium/Neon Hollow-Cathode Reference Lamp in the region 240 - 790 nm.

TPD document, 1994
IFOV measurements of GOME FM, TPD-ERS-GO-MIR-31.